ACS OMEGA

http://pubs.acs.org/journal/acsodf

Article

IRMPD Spectroscopy of Bare Monodeprotonated Genistein, an Antioxidant Flavonoid

Roberto Paciotti, Barbara Chiavarino, Cecilia Coletti,* Debora Scuderi, Nazzareno Re, Davide Corinti, Lucretia Rotari, Simonetta Fornarini, and Maria Elisa Crestoni*

Cite This: *ACS Omega* 2022, 7, 19535−19544

Read Online

ACCESS | Metrics & More | Article Recommendations | Supporting Information

ABSTRACT: Genistein is a naturally occurring polyphenol belonging to the family of flavonoids with estrogenic properties and proven antioxidant, anti-inflammatory, and hormonal effects. Genistein and its derivatives are involved in radical scavenging activity by way of mechanisms based on sequential proton-loss electron transfer. In view of this role, a detailed structural characterization of its bare deprotonated form, $[geni\text{-}H]^-$, generated by electrospray ionization, has been performed by tandem mass spectrometry and infrared multiple photon dissociation (IRMPD) spectroscopy in the 800−1800 cm^{-1} spectral range. Quantum chemical calculations at the B3LYP/6-311+G(d,p) level of theory were carried out to determine geometries, thermochemical data, and anharmonic vibrational properties of low-lying isomers, enabling to interpret the experimental spectrum. Evidence is gathered that the conjugate base of genistein exists as a single isomeric form, which is deprotonated at the most acidic site (7-OH) and benefits from a strong intramolecular H-bond interaction between 5-OH and the adjacent carbonyl oxygen in the most stable arrangement.

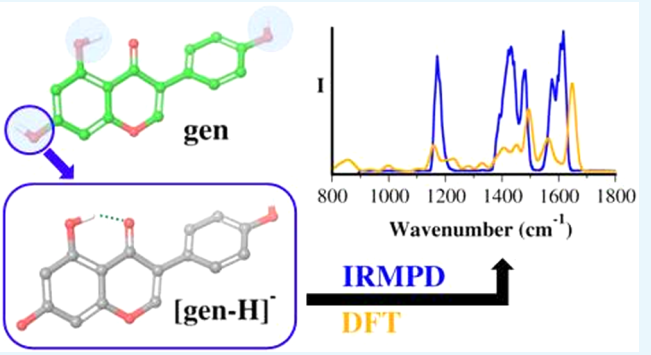

INTRODUCTION

Flavonoids are ubiquitous plant secondary metabolites, exhibiting diverse biological effects.[1] The broad variety of their potential benefits on human health, including antioxidant, anti-inflammatory, antiangiogenic, and anticancer activities,[2,3] is ascribed to the polyphenolic assembly, associated with the function as free-radical scavengers and metal ion chelating agents.[2,4] However, the mechanism by which flavonoids exert their bioactivity is still far from being fully clarified and even a tiny chemical diversity can significantly alter their bioactivity and pharmacokinetics. A class of flavonoids, the isoflavones, are also phytoestrogens, naturally occurring estrogen-like compounds with a structure resembling 17β-estradiol hormones.[5] In particular, genistein (4′,5,7-trihydroxyisoflavone depicted in Figure 1), whose main dietary source is represented by soybeans and legumes, exhibits heart-protective properties, mainly through the reduction of total cholesterol levels and an inhibitory effect on protein kinase with vasodilatation effects. It can also ameliorate painful neuropathy[6] and bind to the estrogen receptor, performing as a safe option for hormone replacement therapy.[7] In recent years, many experimental surveys have addressed the interaction of genistein with free radicals, revealing inter alia an increased scavenging activity upon ultraviolet irradiation.

Theoretical studies have addressed the structure−activity relationship responsible for the role of genistein as a radical scavenger by calculating the reaction enthalpies of antioxidant action mechanisms.[8,9]

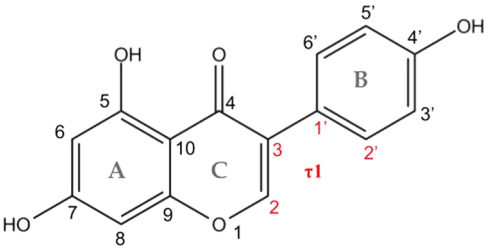

Figure 1. Structure of genistein. The numbering of carbon atoms defining the dihedral angle τ1 (formed by the C2−C3−C1′−C2′ atoms) is reported in red.

The structure of neutral genistein has been investigated using both experimental and computational approaches. A conformational analysis of solid-state genistein carried out by FTIR and Raman spectroscopy has assessed a strong

Received: March 1, 2022
Accepted: May 17, 2022
Published: May 30, 2022

intramolecular H-bond interaction involving 5-OH and the carbonyl oxygen atom arranged in a six-membered ring and a B-ring noncoplanar with the AC-fused rings.[10] Quantum chemical calculations have also assisted spectral assignments in the interpretation of UV/vis, IR/Raman, and 1H/13C NMR absorption spectra of genistein and of the hydrogen-bonded dimer.[11,12]

Besides its potent estrogenic activity, genistein has been reported to exhibit antioxidative properties by scavenging reactive oxygen species, including hydroxyl and superoxide anion radicals and hydrogen peroxide.[13]

Deprotonation of the hydroxyl groups of flavonoids favors their ability as natural metal chelators.[14] Insight into the protective role of polyphenols by sequestering transition-metal ions has been gained by quantum chemical methods determining the acidity at hydroxyl sites. The 4′-position on ring B and 7-position on ring A are considered to be the most favored deprotonation sites, which is ascribed to the enabled higher degree of π-electron delocalization.[15]

Deprotonation has a considerable impact on the radical scavenging activity of flavonoids, rendering it sensitive to solvent polarity.[16] Genistein exists in a monoanionic form at physiological pH.[17] Deprotonated genistein, $[\text{geni-H}]^-$, is a key intermediate in the multistep scheme that accounts for radical scavenging activity (Scheme 1).[18−20] In particular,

Scheme 1. Reaction Scheme for Antioxidant Action in Water via Deprotonated Genistein

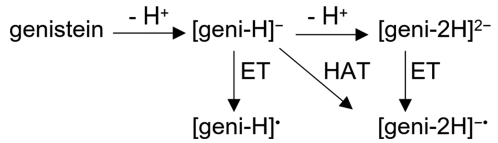

$[\text{geni-H}]^-$ may undergo electron transfer (ET) yielding a phenoxy radical, but it may also undergo a successive proton transfer forming a dianion, which then releases an electron. This latter sequence (sequential proton-loss electron-transfer mechanism) is found to be a favored reaction pathway for deprotonated isoflavones relative to hydrogen atom transfer (HAT) or ET according to density functional theory calculations.[18−20] These computational results shed light on the pH dependence of the antioxidant properties of flavonoids and on the circumstance that the monoanionic form of genistein is a more powerful radical scavenger than the neutral molecule.[17,21] Where deprotonation is unfavored, as in apolar or lipid environments, polyphenols are poor antioxidants.

In this context, to achieve deeper insight into the biochemical activity of genistein, it appears desirable to ascertain the intrinsic bonding and structural features at a molecular level, also aiming to support its unequivocal discrimination from isomeric species. Mass spectrometry-based tools allow us to operate in the gas phase in the absence of external interferences due to the presence of solvent or counterions.

Previous efforts aiming to identify flavonoid glycosides by collision-induced dissociation (CID) mass spectrometry have required complexation by a metal with strong chelating abilities, such as aluminum (III).[22] The focus of the current work is now on bare $[\text{geni-H}]^-$, aiming to clarify its structural features also to possibly implement benchmarking methods for isomeric flavonoid differentiation.

This contribution relies on infrared multiple photon dissociation (IRMPD) spectroscopy in the fingerprint region, which has already offered highly diagnostic information integrating mass spectrometric results.[23−26] Relying on a structure-dependent photofragmentation process induced by the sequential, resonant absorption of multiple IR photons, IRMPD has been exploited to identify the structural and electronic features of a variety of ionic species, including (de)protonated (bio)molecules,[27] reaction intermediates,[28] isomers,[29−31] and metal complexes of amino acids,[32] nucleotides,[33−35] and cofactors.[36]

In addition, quantum chemical calculations have been performed to sample low-energy candidate isomers and to obtain optimized geometrical and electronic structures and linear IR absorption spectra. This inquiry originates from the current, increasing interest in the application of IR spectroscopy as a versatile analytical tool to clarify the structural features of small (bio)molecules involved in relevant metabolic functions.[31,37−41]

METHODS

Sample Preparation. All solvents and reagents, including genistein ($C_{15}H_{10}O_5$) and 4′,5,7-trihydroxyisoflavone (CAS number 446-72-0), were research-grade commercial products (Sigma-Aldrich/Merck, Milan, Italy) used as received. Deprotonated genistein, $[\text{geni-H}]^-$ (m/z 269), was obtained by ESI-MS in a negative ion mode by the direct infusion of a 5 μM methanol solution of genistein, with 2% ammonia to assist deprotonation, at a flow rate of 3 μL min^{-1}.

Mass Spectrometry and IRMPD Spectroscopy. Accurate ion mass measurements were carried out in the cell of a Bruker BioApex Fourier transform ion cyclotron resonance (FT-ICR)[42] mass spectrometer (Bruker Daltonics GmbH, Bremen, Germany), equipped with an Apollo I ESI source, a 4.7 T superconducting magnet (FT-ICR lab, Sapienza Università di Roma), with internal calibration (Δm <2 ppm). CID experiments at variable energies were carried out using a commercial hybrid triple quadrupole linear ion trap mass spectrometer (2000 Q TRAP, Applied Biosystems) with a Q1q2Q_{LIT} configuration (Q1, first mass analyzing quadrupole; q2, nitrogen-filled quadrupole collision cell; and Q_{LIT}, linear ion trap). Electrosprayed $[\text{geni-H}]^-$ ions were mass-selected in Q1, collided with N_2 (nominal pressure of 2.9×10^{-5} mbar) in q2 at variable collision energies (Elab = 5−50 V) for CID experiments, and the dissociation product pattern was monitored by scanning Q_{LIT} in the enhanced mode of operation. Phenomenological threshold energy (TE) values may be derived from the linear extrapolation of the increase of the breakdown curves obtained by plotting the relative abundances of fragment ions as a function of the collision energy, converted to the center of mass frame (ECM = $[m/(m + M)]$Elab, in which m and M are the masses of the collision gas and of the ion, respectively).[43]

IRMPD spectroscopy experiments were carried out in the mid-IR region (800−1800 cm^{-1}) relying on the bright IR radiation of a tunable (5−25 μm) free electron laser (FEL) at the Centre Laser Infrarouge d'Orsay (CLIO)[44] coupled with a hybrid FT-ICR tandem mass spectrometer (Apex-Qe Bruker Daltonics), equipped with a 7.0 T actively shielded magnet and a quadrupole−hexapole interface for mass-filtering and ion accumulation prior to irradiation.[45] Collision-induced dissociation (CID) experiments were also performed in the

https://doi.org/10.1021/acsomega.2c01236
ACS Omega 2022, 7, 19535−19544

quadrupole sector of the instrument at different collision energy (CE) values.

To optimize the laser power at approximately 1.0 W in the explored frequency range, the FEL electron energy was operated at 44.4 MeV. Deprotonated genistein ions (m/z 269) were mass-selected in the quadrupole, collisionally thermalized for 0.4 s with buffer gas (Argon) in the hexapole, and irradiated for 0.55−1.0 s with the IR-FEL light.

The stepwise absorption of multiple resonant photons, combined with fast intramolecular vibrational energy redistribution, can result in a wavelength-dependent photofragmentation process.[46]

IR action spectra are therefore obtained by recording the photofragmentation yield R, defined as $\ln[I_P/(I_P + \sum I_F)]$, where I_P and $\sum I_F$ are the parent and sum of the fragment ion intensities, respectively, as a function of the IR photon energy.[47] At each selected wavenumber, four mass spectra were recorded and averaged.

Computational Methods. Genistein is characterized by three phenolic OH groups, connected to C5, C7, and C4′ atoms. The first two carbon atoms belong to the A-ring (benzopyran scaffold), while C4′ is part of the phenyl B-ring (Figure 1). Potential candidates of $[\text{geni-H}]^-$, deprotonated at either hydroxyl groups, were evaluated in several conformational variants by the systematic stepwise rotation of the routable torsional angles as τ1, C6−C5-O−H, C6−C7-O−H, and C3′−C4′-O−H. Optimized geometries, thermodynamic properties (electronic energy values, zero point energy (ZPE) and thermal corrections, entropies, and free energies at 298 K), and harmonic vibrational frequencies were calculated in the gas phase at the B3LYP/6-311+G(d,p) level of theory.

The lowest-energy structure was used as the input geometry for a preliminary benchmark to identify the best computational settings to quantitatively reproduce the experimental IRMPD signatures. In particular, several DFT functionals were evaluated (other than B3LYP), namely, M06-2X,[48] ωB97XD,[49] LC- ωPBE,[50−52] CAM-B3LYP,[53] and B3LYP-D3,[54,55] for the calculation of the anharmonic frequency corrections with the second-order perturbation theory, VPT2.[56] Only the active modes falling in the range of 800−4000 cm^{-1} (modes 34−81) were included in the calculations.

All of the calculated spectra were obtained using anharmonic unscaled frequencies and harmonic intensities, convoluted assuming a Gaussian profile with an associated width (FWHM) of 15 cm^{-1}.

Geometry optimization and IR frequency calculations, together with the thermodynamic properties (electronic energy values, zero point energy (ZPE) and thermal corrections, entropies, and free energies at 298 K), were also performed in methanol, at the B3LYP/6-311+G(d,p) level of theory, adopting the conductor-like polarizable continuum model (CPCM).[57,58]

The observed fraction of (de)protonated ions may be in fact strongly affected by the spray solvent due to the possible coexistence of isomers in variable ratios in the sampled electrospray ion population.[59−61]

The influence of polar solvents on the enhanced radical scavenging activity of deprotonated genistein has clearly emerged in a study where relevant thermodynamic parameters were re-evaluated by employing a polarized continuum model.[62]

All quantum chemical calculations were performed with the Gaussian09 package.[63]

RESULTS AND DISCUSSION

Photodissociation and CID Mass Spectra. Direct infusion electrospray ionization (ESI) in the negative mode of a methanol solution of genistein delivers a strong signal at m/z 269 due to the conjugate base of genistein, $[\text{geni-H}]^-$, as displayed in the high-resolution mass spectrum of Figure S1, where the monoisotopic peak is revealed at m/z 269.04567, confirming the expected elemental composition, $[C_{15}H_9O_5]^-$. No multiply charged anions, such as $[\text{geni-2H}]^{2-}$, are observed, as expected in view of the known ESI-MS problematics in delivering multiply charged anions from relatively small polyprotic acids.[64] The fragmentation behavior of the mass-selected deprotonated ion, $[\text{geni-H}]^-$, has been assayed by CID experiments.

Figure S2 displays the CID mass spectrum of $[\text{geni-H}]^-$ (m/z 269) obtained in a hybrid triple quadrupole linear ion trap mass spectrometer. Multiple dissociation channels are observed mainly leading to product ions, which imply CO, CO_2, C_2H_2O, and C_2O losses, besides the cross-cleavage of C-ring, as shown in Table S1. In-source CID of $[\text{geni-H}]^-$ ions carried out in the FT-ICR mass spectrometer has enabled the identity of these fragments to be verified by measuring the mass accuracy achieved with a confidence of ±1.0 ppm. The appearance of competitive and sequential fragmentation paths has also been examined by CID at variable resonance excitation amplitude and verified by MS^3 experiments in a triple quadrupole mass spectrometer, as shown in the breakdown graphs of Figure S3, where the abundances of secondary products are clustered together with their respective precursor. Although quantitative threshold values are not directly accessible,[65] nevertheless phenomenological threshold energies (TEs) of the various fragmentation routes may be obtained for a comparative analysis among competitive dissociation pathways. Linear extrapolation of the increase of the breakdown curves delivers TE values of 1.4−1.7 eV for the appearance of m/z 241, 240, 227, and 225, indicating the loss of CO-containing small molecules as the lowest-energy fragmentation routes. The products of C-ring cleavage are formed at higher energies: the $^{0,3}A^-$ (m/z 135) and $^{0,3}B^-$ (m/z 133) ionic species, where the left superscripts denote the broken C-ring bonds, appear at ca. 2.4 eV and the $^{1,3}A^-$ (m/z 151) and $^{1,3}B^-$ (m/z 117) products are found for a center of mass energy in excess of 3.7 eV (Table S1).

Accordingly, a plausible fragmentation scheme is presented in Figure S4.

These outcomes are consistent with previous reports on various flavonoid aglycones[66] and on the anion (m/z 269) generated at low collision energies from deprotonated genistein−7-O-glucoside by a hydroxyl atom rearrangement process.[67] Although unusual neutral losses involving CO, CO_2, and C_3O_2 were shown to be characteristic of negative ion mode, thus complementing some diagnostic ions observed in positive polarity, still a higher structural specificity is required to differentiate isomeric flavonoids in the phytochemical screening of complex mixtures. In this context, an effort that combines MS coupled to IRMPD spectroscopy is applied here to provide more distinctive clues to characterize genistein.

A similar fragmentation pattern, with comparable branching ratio, is also obtained when the parent ion (m/z 269) is probed by resonant IR excitation to elucidate vibrational and molecular features using the IR-FEL at CLIO in the mid-IR domain (850−1900 cm^{-1}). An exemplary mass spectrum

https://doi.org/10.1021/acsomega.2c01236
ACS Omega 2022, 7, 19535−19544

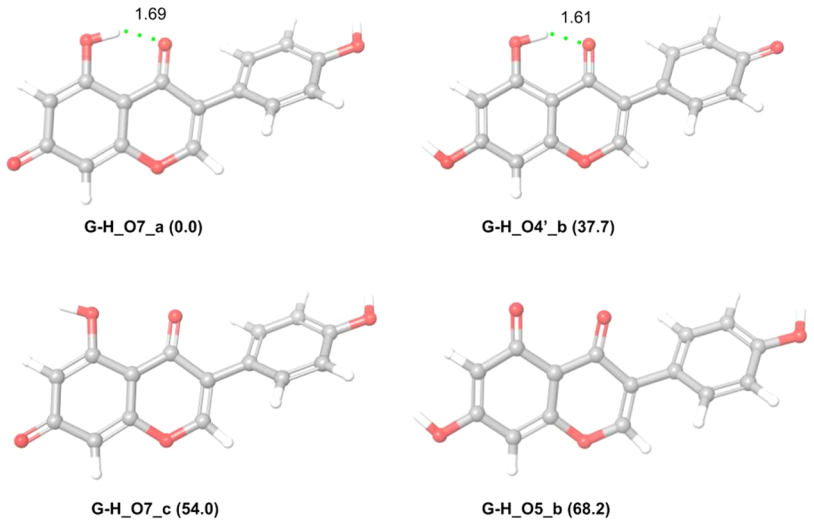

Figure 2. Optimized geometries of the lowest-energy isomers and conformers of deprotonated genistein computed in the gas phase at the B3LYP/6-311+G(d,p) level of theory. Relative free energies are reported in parentheses in kJ mol^{-1}, and intramolecular hydrogen-bond distances (green dashed lines) are reported in Å.

recorded when [geni-H]$^-$ ions are exposed to the CLIO FEL light on resonance at 1605 cm^{-1} is shown in Figure S5. This evidence conforms to both methods that favor a slow heating process, with subsequent dissociation along the lowest-energy channel.[46]

Computational Survey. A computational study was performed to identify the most stable structures of the genistein anion, i.e., phenate isomers deprotonated either at 7-OH, 5-OH, or 4′-OH hydroxyl groups on the aromatic rings (A and B) and their conformational variants differing in the OH orientation. Theoretical IR frequencies are also required to interpret the experimental IRMPD spectrum, which mainly reveals the absorption of the first resonant IR photon. The four lowest-energy structures of [geni-H]$^-$ are shown in Figure 2, together with their relative free energies in kJ mol^{-1}, while other low-lying isomers and conformers are reported in Figure 3. A complete list of the relative free-energy and enthalpy values of each isomer/conformer, together with the values of the torsional angle τ1 identified between the planes of AC and B rings (Figure 1), is provided in Table S2.

The lowest-lying isomer, **G-H_O7_a**, results from deprotonation of 7-OH and benefits from a strong intramolecular H bond between 5-OH and the adjacent C4 carbonyl oxygen ($r_{SOH\cdots O=C}$ = 1.69 Å). When such an interaction is hampered by a 180° rotation around C5-OH, conformer **G-H_O7_c** is found to lie 54.0 kJ mol^{-1} higher in energy. This indicates a significant contribution of this contact to the molecule stability, in agreement with the published data.[68,69] Conversely, a 180° rotation of C4′-OH has little influence on relative energies, yielding conformer **G-H_O7_b**, only 1.1 kJ/mol higher in energy (Figure 3). The dihedral angle τ1 is −38.9 ° in the global minimum (−40.2° in conformer **G-H_O7_b**; Table S2) and −42.8 °in neutral genistein,[68] indicating that deprotonation leads to a reduction of the inter-ring torsional angle.[68] This trend is even more evident when deprotonation affects 4′-OH (B-ring) as in **G-H_O4′_b**, which is placed 37.7 kJ mol^{-1} above **G-H_O7_a** and shows the lowest value computed for this dihedral angle (τ1 = −29.9 °) (Table S2) and a shorter intramolecular H bond ($r_{SOH\cdots O=C}$ = 1.61 Å). A 180° rotation of C7-OH leads to **G-H_O4′_a**, only 0.7 kJ mol^{-1} higher in energy (Figure 3 and Table S2).

Deprotonation at 5-OH (A-ring) generates isomer **G-H_O5_b**, at 68.2 kJ mol^{-1} relative energy, characterized by the obvious lack of the stabilizing intramolecular H bond and by a τ1 value equal to −40.2°.

The τ1 values presently obtained for **G-H_O7_a**, **G-H_O4_b**, and **G-H_O5_b** in the gas phase are in agreement with previous computations on neutral genistein.[68]

For the sake of completeness, other [geni-H]$^-$ isomers were obtained by considering a hydrogen atom placed on the C4 carbonyl oxygen (heterocyclic C-ring), as displayed in Figure 3. Consequently, in **G-H_OH4_OH5_a** (82.1 kJ mol^{-1}), **G-H_O4′_OH4_a** (109.6 kJ mol^{-1}), and **G-H_O7_OH4_a** (157.0 kJ mol^{-1}), the 4-OH moiety can establish a H bond with the π system of the B-ring. To maximize this contact, a significant increase of τ1 occurs with values of −53.5 °, −51.1°, and −55.0°, respectively. Conversely, in **G-H_OH4_OH5_b** (110.6 kJ mol^{-1}), where both 5-OH and 4-OH are rotated by 180°, τ1 decreases to −36.4° because no H bond with the B-ring can be formed.

As shown in Table S3, the analysis of the relative free energies of genistein anions computed in methanol confirms the same trend found in the gas phase, albeit with some differences. For instance, the conformer pairs **G-H_O7_a**/**G-H_O7_b** (deprotonated A-ring) and **G-H_O4′_a**/**G-H_O4′_b** (deprotonated B-ring) are characterized by very close free-energy values (within the chemical accuracy), and the passage from gas to methanol phase only affects the relative stability of the highest-energy structures, as **G-H_O4′_c**, **G-H_O4′_OH4_a**, and **G-H_O7_OH4_a**, namely, those lacking an intramolecular H bond. Among the latter structures, the **G-H_O4′_c** isomer presents relatively more exposed hydroxyl groups, this gaining the larger stabilization from methanol solvent. Furthermore, the presence of the solvent does not significantly affect the $r_{SOH\cdots O=C}$ distances, while τ1 value is increased (more negative) in each isomer/conformer with respect to the corresponding gas-phase structure (Table S3).

The analysis of the relative free energies indicates that the stability of genistein anions follows the order 7-OH > 4′-OH > 5-OH. The species obtained by deprotonation of 7-OH is the most stable isomer in both gas and methanol phases. According to the literature,[68] this trend follows the order of

https://doi.org/10.1021/acsomega.2c01236
ACS Omega 2022, 7, 19535−19544

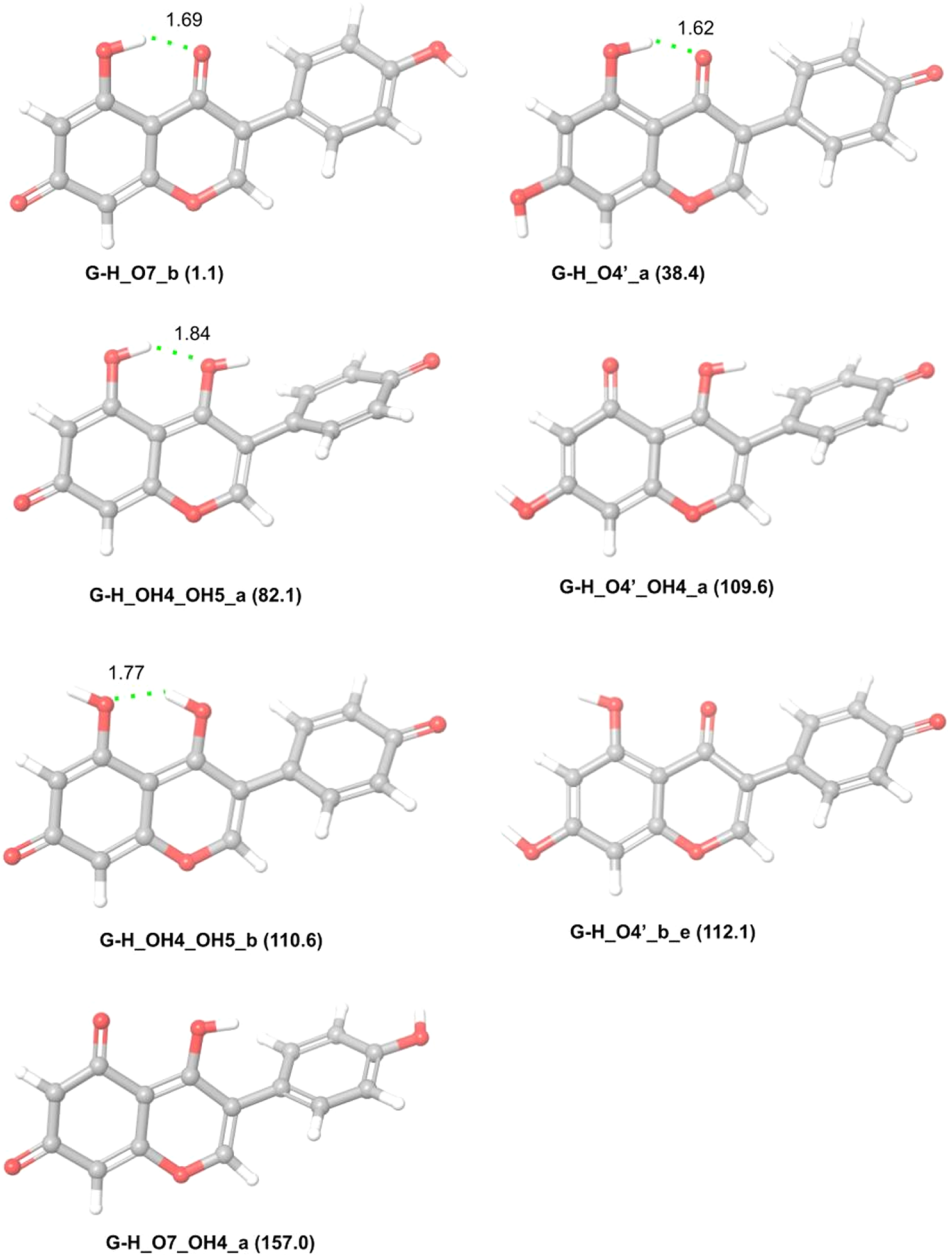

Figure 3. Optimized geometries of isomers and conformers of deprotonated genistein computed in the gas phase at the B3LYP/6-311+G(d,p) level of theory. Relative free energies are reported in parentheses in kJ mol^{-1}, and intramolecular hydrogen-bond distances (green dashed lines) are reported in Å.

proton affinity values of 7-OH, 4′-OH, and 5-OH for genistein anions calculated at the B3LYP/6-311++G(2d,2p) level of theory. Those results can easily be employed to derive the corresponding relative enthalpies, which fully agree with the present results (Table S4).

A different trend of proton affinity values (7-OH, 5-OH, and 4′-OH) was instead computed in the gas phase using the B3LYP/6-31+G(d,p)//B3LYP/6-311++G(d,p) level of theory,[70] suggesting that a triple-zeta quality basis set is necessary to accurately reproduce the energy contribution of the 5-OH···O═C hydrogen bond and therefore the relative stability of $[geni\text{-}H]^-$ derivatives (Table S4).

The deprotonation site also affects the electrostatic potential of the corresponding genistein anions, as shown in Figure S6, and in **G-H_O7_a**, the negative charge is mainly localized on the C7−C8−C9 atoms (A-ring).

The vibrational modes of moieties involved in intramolecular interactions detected in $[gen\text{-}H]^-$ derivatives can be characterized by a highly anharmonic behavior. The theoretical evaluation of the corresponding IR wavenumbers may benefit from the use of functionals including long-range and dispersion corrections and from the calculation of anharmonic frequencies, as indicated by a recent assessment of commonly used DFT functionals in reproducing structural parameters[71] and IRMPD signatures of intramolecular H-bonded ions.[72] Therefore, a preliminary benchmark study was performed to evaluate the behavior of M06-2X, ωB97XD, LC-ωPBE, CAM-B3LYP, B3LYP-D3, and B3LYP functionals with the 6-311+G(d,p) basis set.

https://doi.org/10.1021/acsomega.2c01236
ACS Omega 2022, 7, 19535−19544

As shown in Figure S7, the anharmonic frequencies computed with B3LYP-D3 and B3LYP provide the best quantitative matching with the experimental IRMPD signatures, as found for other classes of compounds.[56]

Interestingly, the anharmonic (as well as the harmonic) vibrational frequencies computed with B3LYP and B3LYP-D3 are almost equivalent, in agreement with a study by Barone and co-workers showing that both B3LYP and B3LYP-D3 provide the highest accuracy for the prediction of vibrational frequencies of isolated monomers, whereas B3LYP-D3 gives the best results for stacked dimers.[73] Therefore, the B3LYP/6-311+G(d,p) level of theory has been used here to obtain the anharmonic frequencies for the spectral assignment of [geni-H]$^-$.

Spectral Assignment. The IRMPD spectrum of [geni-H]$^-$ is characterized by two prominent, only partially resolved absorptions centered at 1576 and 1617 cm^{-1} and at 1429 and 1483 cm^{-1} by a sharp resonance at 1171 cm^{-1}. In addition, barely noticeable shoulders may be located at 1399, 1448, and 1605 cm^{-1} (Figure 4).

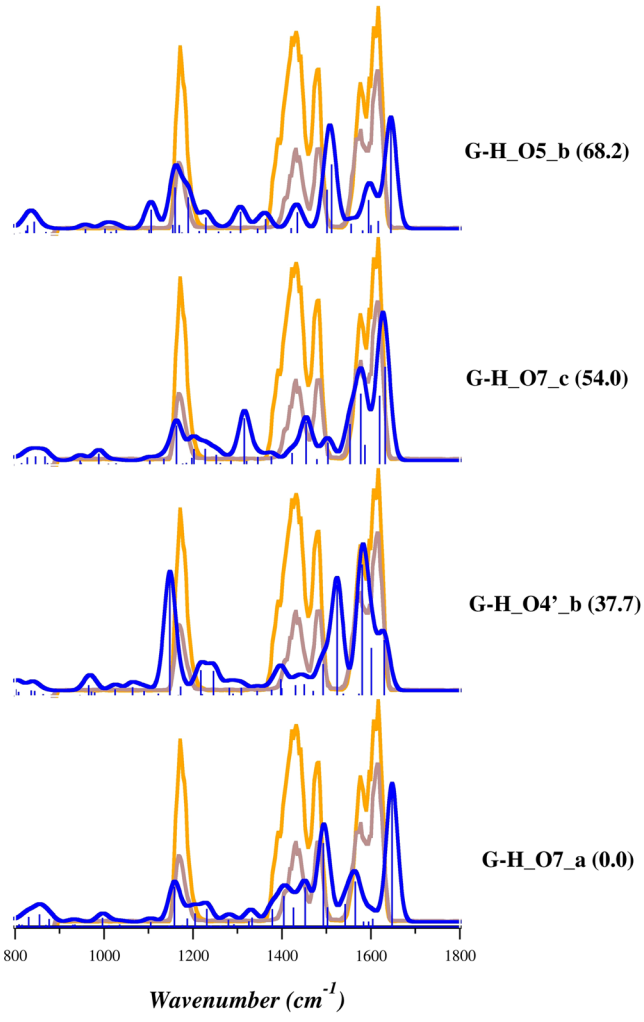

Figure 4. IRMPD spectrum (orange and magenta profiles) and the calculated anharmonic IR spectra (blue profiles) of the lowest-lying conformers and isomers of deprotonated genistein computed at the B3LYP/6-311+G(d,p) level of theory in the gas phase. Free energies relative to **G-H_O7_a** are reported in parentheses (kJ mol^{-1}).

For structural and spectral assignments, the experimental IRMPD spectrum of the conjugate base of genistein has been compared with the calculated IR spectra of the low-lying isomers **G-H_O7_a**, **G-H_O4′_b**, and **G-H_O5_b** and the **G-H_O7_c** conformer in the 800−1800 cm^{-1} range (Figure 4). The position of the main IRMPD absorptions and the computed anharmonic IR bands of the global minimum **G-H_O7_a** are listed in Table 1, together with relative intensities (in parentheses) and a brief mode description. In addition, a thorough presentation of the linear IR spectra of all identified structures is presented in Figures S8 and S9, while their calculated vibrational frequencies and assigned modes are described in Tables S5−S15.

The comparative assessment of Figures 4 and S8 uncovers that the main IRMPD features of [geni-H]$^-$ ion find the best overall match with the absorptions of the lowest-energy geometry, **G-H_O7_a**, consistent with a predominant contribution of the isomer deprotonated at the 7-OH hydroxyl (A-ring), favored both in solution and in the gas phase. Due to the proximity in energy and the almost identical IR spectrum of its **G-H_O7_b** rotamer (Figure S8), an admixture of contributing lowest-energy species is likely present in the ESI-sampled ion population.

In particular, the two prominent, partially resolved peaks at 1617 and 1576 cm^{-1} may be associated with a combination of the molecular deformations (A+C rings) and the C5-OH in plane bending predicted at 1648 cm^{-1} and with the C4═O and the C7-O stretching modes, the latter being a signature of the deprotonation site, expected at 1565 cm^{-1}. Noteworthily, the shape of this envelope may arise from the multiple photon nature of the method, where a weak band (1565 cm^{-1}) on the red side of a strong resonance (1617 cm^{-1}) acquires an increased activity. The ensemble of intense bands between 1360 and 1500 cm^{-1} satisfactorily matches with (i) the C5-OH bending coupled with C4═O stretch and C-Hs bending (B-ring) calculated at 1493 cm^{-1}; (ii) the C5-OH bending and molecular deformations (A + C rings) computed at 1452 cm^{-1}; (iii) the CHs rocking (B-ring) expected at 1426 cm^{-1}; and (iv) the C5-OH bending calculated at 1404 cm^{-1}. Finally, the strong absorbance at 1171 cm^{-1} is well interpreted by the C4′-OH bending at 1158 cm^{-1} merging with the C5-OH stretch at 1187 cm^{-1} for **G-H_O7_a**. The former peak is obviously missing in the linear IR spectrum of the less stable isomer **G-H_O4′_b**.

A relevant contribution of the latter structure, **G-H_O4′_b**, can be ruled out also based on the C5-OH bending coupled with the C4═O stretch and molecular deformation, which is blue-shifted at 1524 cm^{-1}, where the IRMPD spectrum appears remarkably flat. Moreover, the weak activity predicted in the 1370−1480 cm^{-1} range, ascribable to molecular deformation modes that include the diagnostic C4′-O stretch at 1450 cm^{-1}, is not consistent with the experimental evidence, while the resonance at 1148 cm^{-1}, due to CHs rocking, does not guarantee an enhanced agreement with the IRMPD spectrum (Table S6). Similarly, the relatively higher-energy **G-H_O7_c** conformer, where the 180° rotation around the C5-OH bond noticeably destabilizes this geometry relative to the **G-H_O7_a** arrangement, shows an intense band at 1316 cm^{-1}, corresponding to the C2-H bending and molecular deformation, which is not consistent with experimental evidence. In **G-H_O7_c**, the absence of an intramolecular hydrogen bond gives rise to both a blue shift of the C5-OH and C4═O stretching modes to 1202 and 1578 cm^{-1}, respectively, and of

https://doi.org/10.1021/acsomega.2c01236
ACS Omega 2022, 7, 19535−19544

Table 1. Observed IRMPD Resonances and Theoretical Anharmonic IR Frequencies and Normal Vibrational Modes for the Four Lowest-Energy Genistein Anions (G-H_O7_a, G-H_O4′_b, G-H_O7_c, and G-H_O5_b) Obtained from DFT Calculations at the B3LYP/6-311+G(d,p) Level in the Gas Phase[a]

Theoretical anharmonic frequency[b,c] (intensity)[d] *vibrational mode description*[e]				
G-H_O7_a	G-H_O4′_b	G-H_O7_c	G-H_O5_b	IRMPD[b]
1158 (288) *δ 4′-OH*	**1148 (864)** *ρ* C-H phenol	**1163 (284)** *δ 4′-OH*	**1160 (338)** *δ 4′-OH*	**1171**
1187 (54) *ν 5-OH*	**1172(65)** *δ* C6-H		**1189 (264)** *δ* C6-H and C8-H, mol. def. *δ 4′-OH*	
1404 (221) *δ 5-OH*	**1397 (120)** *ρ* C-H B-ring	**1376 (57)** mol. def.	**1364 (104)** *ν C9-O1*, *δ* 7-OH, mol. def.	**1399**
	1399 (53) mol. def., *δ 5-OH*			
1426 (136) *ρ* C-H (B-ring)	**1431(75)** mol. def.	**1423 (84)** *δ 4′-OH*, mol. def.	**1435 (155)***ν* C9-C10, *δ* C6-H and C8-H, mol. def.	**1429**
1452 (285) *δ 5-OH*, mol. def.	**1450 (82)** *mol. def.*, *ν C4′-O*	**1454 (310)** *ν C5-OH*, mol. def.		**1448**
1493 (609) *δ 5-OH*, *ν C4═O*	**1493 (231)** *δ* 5-OH, mol. def.	**1504 (60)** *δ 4′*-OH	**1501 (320)** *ν C3-C1′*, *ν C4′-OH*, *δ* C-H phenol	**1483**
	1524 (814) *ν* C4═O, *δ* 5-OH, mol. def.		**1512 (507)** *ν* C4═O, *ν* C5═O, mol. def.	
1565 (327) *ν* C4═O, *ν* C7-O, *δ* 5-OH, mol. def	**1580 (963)** *ν* C4═O, *ν* C4′-O	**1553 (297)** *δ* 5-OH, *ν* C7-O, mol. def.	**1556 (70)** *ν* C4═O, *ν* C5═O, mol. def.	**1576**
		1578 (520) *ν* C4═O, mol. def.	**1595 (245)** *ν* C4═O, *ν* C5═O, mol. def.	
		1587 (143) mol. def., *δ* 4′-OH		
1648 (1019) *δ* 5-OH, mol. def. (A + C) rings	**1630 (406)** *δ* 5-OH, mol. def	**1620 (504)** *ν* C4═O, *δ* 5-OH, mol. def	**1617 (91)** *ν* C4═O, mol. def.	**1617**
		1632 (718) *ν* C4═O, *δ* 5-OH, mol. def.	**1645 (813)** *ν* C4═O, *ν* C5═O, mol. def.	

[a]The complete description of the theoretical anharmonic vibrational modes is provided in Tables S5−S8 for each species. [b]In cm^{-1}. [c]Unscaled frequencies. [d]In km mol^{-1}. [e]*ν*: stretching; *δ*: bending; *ω*: wagging; *ρ*: rocking; *mol. def.*: molecular deformation.

the C5-OH bend combined with the C4═O stretch and molecular deformation to 1620 and 1632 cm^{-1}, whereas the C5-OH bending is red-shifted to 1252 cm^{-1}, thus confirming the significant sensitivity of these resonances to the H-bonding network (Table S7).

Deprotonation at the 5-OH hydroxyl functionality leads to the higher-lying **G-H_O5_b** isomer whose IR spectrum is characterized by strong discrepancies, including the intense, diagnostic C5-O stretch at 1512 cm^{-1} and the C2-H and C8-H bending modes at 1307 and 1106 cm^{-1}, respectively, which all are missing in the experimental spectrum, thus disproving its presence in the assayed population (Table S8).

Any significant contribution of higher-energy structures can be ruled out on an energetic basis and inconsistency with the IRMPD spectrum (Figures S8 and S9).

As previously reported, the occurrence of a shared proton-binding motif, such as that engaging 5-OH in the most stable GH_O7 and GH_O4′ structures of [geni-H]$^-$, magnifies the anharmonic behavior of the involved OH bending and related coupled modes.[74] In such cases, where the proton is shared between comparably strong conjugate bases, the standard approach, i.e., the use of a scaling factor to correct harmonic frequencies, would only result in a shifting of the whole spectrum, not helping with the correct vibration assignment. The explicit calculation of anharmonic corrections is therefore mandatory to obtain the desired quantitative accuracy, most often without resorting to additional empirical scaling factors (Figure S10).

The higher (2800−3800 cm^{-1}) wavenumber range encompassing OH stretching modes, which can be accessed by IRMPD spectroscopy, might contribute to clarify the deprotonation site of [geni-H]$^-$. However, a careful examination of the calculated IR spectra (Figure S11) of the four most indicative structures (**G-H_O7_a**; **G-H_O4′_b**; **G-H_O7_c**; **G-H_O5_b**) has shown that (i) the free OH stretches of the all-named isomers are active at the same wavenumber (3630 cm^{-1}) and therefore are not structurally diagnostic absorptions; (ii) all absorptions in this range are characterized by rather low intensity (below 50 km/mol), possibly below the threshold value for their appearance (this nonlinear behavior of IRMPD spectroscopy is well documented and discussed); and (iii) at 2941 cm^{-1}, a highly active mode (375 km/mol) is indeed predicted for the most stable isomer **G-H_O7_a**. Yet, this band pertains to the stretching mode of the C5O-H bond involved in a strong H bond with the nearby O4′ atom of the carbonyl group. As previously reported, the presence of a hydrogen-bond interaction accounts for a remarkable red shift (out of accessible experimental range) and dramatic broadening, frequently leading to a poorly detectable peak in the experimental spectrum. Based on these considerations, exploring the high-energy portion of the spectrum was not deemed significant.

CONCLUSIONS

A detailed structural picture of the conjugate base of genistein, a natural flavonoid with recognized biological activity, has been attained by vibrational spectroscopy in the fingerprint range, CID experiments, and theoretical calculations at the B3LYP/6-311+G(d,p) level. This study was aimed to ascertain the impact of deprotonation on the energetic and geometric features of the bare anion, [geni-H]$^-$, a key intermediate involved in antioxidant mechanisms of polyphenols in polar environments.

The collected evidence reveals that the deprotonation at the resorcinol 7-OH hydroxyl, the thermodynamically most acidic site, provides the lowest-energy structure characterized by (i) an increased electron density at the A-ring but still stabilized by an intramolecular H bond between the phenolic 5-OH and

https://doi.org/10.1021/acsomega.2c01236
ACS Omega 2022, 7, 19535−19544

carbonyl groups and (ii) a decreased inter-ring torsional angle relative to neutral genistein. An admixture of two close-lying rotamers (**GH_07_b** and **GH_07_a**) is found to mainly contribute to the sampled ion population, likely indicating the equilibrium in solution.

Overall, the present study provides spectroscopic signatures of deprotonated genistein potentially useful to relate the direct structural characteristics to biological activity as well as to assist in the analysis of related polyphenol compounds in biological matrices.

■ ASSOCIATED CONTENT

Supporting Information

The Supporting Information is available free of charge at https://pubs.acs.org/doi/10.1021/acsomega.2c01236.

Figures of mass spectra, fragmentation scheme, calculated electrostatic potential, IRMPD profiles, calculated IR spectra, and optimized geometries and tables of IRMPD absorptions and calculated vibrational frequencies (PDF)

■ AUTHOR INFORMATION

Corresponding Authors

Cecilia Coletti − *Dipartimento di Farmacia, Università G. D'Annunzio Chieti-Pescara, Chieti I-66100, Italy;* orcid.org/0000-0002-3609-290X; Email: ccoletti@unich.it

Maria Elisa Crestoni − *Dipartimento di Chimica e Tecnologie del Farmaco, Università di Roma "La Sapienza", I-00185 Roma, Italy;* orcid.org/0000-0002-0991-5034; Email: mariaelisa.crestoni@uniroma1.it

Authors

Roberto Paciotti − *Dipartimento di Farmacia, Università G. D'Annunzio Chieti-Pescara, Chieti I-66100, Italy;* orcid.org/0000-0001-5325-9452

Barbara Chiavarino − *Dipartimento di Chimica e Tecnologie del Farmaco, Università di Roma "La Sapienza", I-00185 Roma, Italy;* orcid.org/0000-0002-1585-7061

Debora Scuderi − *Institut de Chimie Physique (UMR8000), CNRS, Université Paris-Saclay, 91405 Orsay, France*

Nazzareno Re − *Dipartimento di Farmacia, Università G. D'Annunzio Chieti-Pescara, Chieti I-66100, Italy;* orcid.org/0000-0002-0957-4049

Davide Corinti − *Dipartimento di Chimica e Tecnologie del Farmaco, Università di Roma "La Sapienza", I-00185 Roma, Italy;* orcid.org/0000-0001-8064-3492

Lucretia Rotari − *Dipartimento di Chimica e Tecnologie del Farmaco, Università di Roma "La Sapienza", I-00185 Roma, Italy;* orcid.org/0000-0001-5086-7487

Simonetta Fornarini − *Dipartimento di Chimica e Tecnologie del Farmaco, Università di Roma "La Sapienza", I-00185 Roma, Italy;* orcid.org/0000-0002-6312-5738

Complete contact information is available at: https://pubs.acs.org/10.1021/acsomega.2c01236

Notes

The authors declare no competing financial interest.

■ ACKNOWLEDGMENTS

This work was funded by the Italian Ministry for University and Research, Dipartimenti di Eccellenza, L. 232/2016, and by the European Union's Horizon 2020 research and innovation program under grant agreement Nos. 731077 (EU_FT-ICR_MS) and 730872 (CALIPSO plus). Financial support from the National FT-ICR network (FR 3624 CNRS) for conducting the research was gratefully acknowledged. The authors gratefully acknowledge Philippe Maitre, Estelle Loire, Jean-Michel Ortega, and the CLIO team for valuable assistance.

■ REFERENCES

(1) Dixon, R. A.; Steele, C. L. Flavonoids and Isoflavonoids − a Gold Mine for Metabolic Engineering. *Trends Plant Sci.* **1999**, *4*, 394−400.

(2) Kopustinskiene, D. M.; Jakstas, V.; Savickas, A.; Bernatoniene, J. Flavonoids as Anticancer Agents. *Nutrients* **2020**, *12*, 457.

(3) Sychrová, A.; Kolářiková, I.; Žemlička, M.; Šmejkal, K. Natural Compounds with Dual Antimicrobial and Anti-Inflammatory Effects. *Phytochem. Rev.* **2020**, *19*, 1471−1502.

(4) Dixon, R. A.; Pasinetti, G. M. Flavonoids and Isoflavonoids: From Plant Biology to Agriculture and Neuroscience. *Plant Physiol.* **2010**, *154*, 453−457.

(5) Yearley, E. J.; Zhurova, E. A.; Zhurov, V. V.; Pinkerton, A. A. Binding of Genistein to the Estrogen Receptor Based on an Experimental Electron Density Study. *J. Am. Chem. Soc.* **2007**, *129*, 15013−15021.

(6) Valsecchi, A. E.; Franchi, S.; Panerai, A. E.; Sacerdote, P.; Trovato, A. E.; Colleoni, M. Genistein, a Natural Phytoestrogen from Soy, Relieves Neuropathic Pain Following Chronic Constriction Sciatic Nerve Injury in Mice: Anti-Inflammatory and Antioxidant Activity. *J. Neurochem.* **2008**, *107*, 230−240.

(7) Desmawati, D.; Sulastri, D. A Phytoestrogens and Their Health Effect. *Open Access Maced. J. Med. Sci.* **2019**, *7*, 495−499.

(8) Zhang, H.-Y.; Wangb, L.; You-Min Sunc, Y. Why B-Ring is the Active Center for Genistein to Scavenge Peroxyl Radical: A DFT Study. *Bioorg. Med. Chem. Lett.* **2003**, *13*, 909−911.

(9) Lengyel, J.; Rimarčík, J.; Vagánekc, A.; Klein, E. On the radical scavenging activity of isoflavones: thermodynamics of O−H bond cleavage. *Phys. Chem. Chem. Phys.* **2013**, *15*, 10895−10903.

(10) Machado, N.F.L.; Batista de Carvalho, L.A.E.; Otero, J. C.; Marques, M.P.M. A conformational study of hydroxylated isoflavones by vibrational spectroscopy coupled with DFT calculations. *Vibr. Spectrosc.* **2013**, *68*, 257−265.

(11) Singh, R. K.; Singh, A. K. DFT calculations on molecular structure, spectral analysis, multiple interactions, reactivity, NLO property and molecular docking study of flavanol-2,4-dinitrophenylhydrazone. *J. Mol. Struct.* **2017**, *1129*, 128−141.

(12) Zielińska, A.; Paradowska, K.; Jakowski, J.; Wawer, I. ^{13}C CP MAS NMR and GIAO-CHF/DFT calculations of flavonoids: Morin, kaempferol, tricin, genistein, formononetin and 3,7-dihydroxyflavone. *J. Mol. Struct.* **2008**, *873*, 109−116.

(13) Kładna, A.; Berczynski, P.; Kruck, I.; Piechowska, T.; Aboul-Enein, H. Y. Studies on the antioxidant properties of some phytoestrogens. *Luminescence* **2016**, *31*, 1201−1206.

(14) Dowling, S.; Regan, F.; Hughes, H. The characterization of structural and antioxidant properties of isoflavone metal chelates. *J. Inorg. Biochem.* **2010**, *104*, 1091−1098.

(15) Leopoldini, M.; Russo, N.; Toscano, M. The Molecular Basis of Working Mechanism of Natural Polyphenolic Antioxidants. *Food Chem.* **2011**, *125*, 288−306.

(16) Caicedo, C.; Iuga, C.; Castañeda-Arriaga, R.; Alvarez-Idaboy, J. R. Antioxidant activity of selected natural polyphenolic compounds from soybean via peroxylradical scavenging. *RSC Adv.* **2014**, *4*, 38918−38930.

(17) Zielonka, J.; Gębicki, J.; Grynkiewicz, G. Radical scavenging properties of genistein. *Free Rad. Biol. Med.* **2003**, *35*, 958−965.

(18) Klein, E.; Rimarčík, J.; Senajová, E.; Vagánek, A.; Lengyel, J. Deprotonation of flavonoids severely alters the thermodynamics of the hydrogen atom transfer. *Comput. Theor. Chem.* **2016**, *1085*, 7−17.

(19) Biela, M.; Rimarčík, J.; Senajová, E.; Kleinová, A.; Klein, E. Antioxidant action of deprotonated flavonoids: Thermodynamics of sequential proton-loss electron-transfer. *Phytochemistry* **2020**, *180*, No. 112528.
(20) Biela, M.; Kleinová, A.; Klein, E. Thermodynamics of radical scavenging effect of deprotonated isoflavones in aqueous solution. *J. Mol. Liq.* **2022**, *345*, No. 117861.
(21) Musialik, M.; Kuzmicz, R.; Pawlowski, T. S.; Litwinienko, G. Acidity of hydroxyl groups: an overlooked influence on antiradical properties of flavonoids. *J. Org. Chem.* **2009**, *74*, 2699−2709.
(22) Zhang, J.; Wang, J.; Brodbelt, J. S. Characterization of Flavonoids by Aluminum Complexation and Collisionally Activated Dissociation. *J. Mass Spectrom.* **2005**, *40*, 350−363.
(23) Fridgen, T. D. Infrared Consequence Spectroscopy of Gaseous Protonated and Metal Ion Cationized Complexes. *Mass Spectrom. Rev.* **2009**, *28*, 586−607.
(24) Polfer, N. C.; Oomens, J. Vibrational Spectroscopy of Bare and Solvated Ionic Complexes of Biological Relevance. *Mass Spectrom. Rev.* **2009**, *28*, 468−494.
(25) Jašíková, L.; Roithová, J. Infrared Multiphoton Dissociation Spectroscopy with Free-Electron Lasers: On the Road from Small Molecules to Biomolecules. *Chem. - Eur. J.* **2018**, *24*, 3374−3390.
(26) Corinti, D.; Paciotti, R.; Re, N.; Coletti, C.; Chiavarino, B.; Crestoni, M. E.; Fornarini, S. Binding Motifs of Cisplatin Interaction with Simple Biomolecules and Aminoacid Targets Probed by IR Ion Spectroscopy. *Pure Appl. Chem.* **2020**, *92*, 3−13.
(27) Corinti, D.; Crestoni, M. E.; Fornarini, S.; Pieper, M.; Niehaus, K.; Giampà, M. An Integrated Approach to Study Novel Properties of a MALDI Matrix (4-Maleicanhydridoproton Sponge) for MS Imaging Analyses. *Anal. Bioanal. Chem.* **2019**, *411*, 953−964.
(28) Roithová, J. Characterization of Reaction Intermediates by Ion Spectroscopy. *Chem. Soc. Rev.* **2012**, *41*, 547−559.
(29) Martens, J.; Koppen, V.; Berden, G.; Cuyckens, F.; Oomens, J. Combined Liquid Chromatography-Infrared Ion Spectroscopy for Identification of Regioisomeric Drug Metabolites. *Anal. Chem.* **2017**, *89*, 4359−4362.
(30) Lepere, V.; Le Barbu-Debus, K.; Clavaguéra, C.; Scuderi, D.; Piani, G.; Simon, A.-L.; Chirot, F.; MacAleese, L.; Dugourd, P.; Zehnacker, A. Chirality-Dependent Structuration of Protonated or Sodiated Polyphenylalanines: IRMPD and Ion Mobility Studies. *Phys. Chem. Chem. Phys.* **2016**, *18*, 1807−1817.
(31) Corinti, D.; Chiavarino, B.; Spano, M.; Tintaru, A.; Fornarini, S.; Crestoni, M. E. Molecular Basis for the Remarkably Different Gas-Phase Behavior of Deprotonated Thyroid Hormones Triiodothyronine (T3) and Reverse Triiodothyronine (RT3): A Clue for Their Discrimination? *Anal. Chem.* **2021**, *93*, 14869−14877.
(32) Boles, G. C.; Hightower, R. L.; Berden, G.; Oomens, J.; Armentrout, P. B. Zinc and Cadmium Complexation of L-Threonine: An Infrared Multiple Photon Dissociation Spectroscopy and Theoretical Study. *J. Phys. Chem. B* **2019**, *123*, 9343−9354.
(33) Cheng, R.; Martens, J.; Fridgen, T. D. A Vibrational Spectroscopic and Computational Study of Gaseous Protonated and Alkali Metal Cationized G−C Base Pairs. *Phys. Chem. Chem. Phys.* **2020**, *22*, 11546−11557.
(34) Zhu, Y.; Roy, H. A.; Cunningham, N. A.; Strobehn, S. F.; Gao, J.; Munshi, M. U.; Berden, G.; Oomens, J.; Rodgers, M. T. IRMPD Action Spectroscopy, ER-CID Experiments, and Theoretical Studies of Sodium Cationized Thymidine and 5-Methyluridine: Kinetic Trapping During the ESI Desolvation Process Preserves the Solution Structure of $[Thd+Na]^+$. *J. Am. Soc. Mass Spectrom.* **2017**, *28*, 2423−2437.
(35) Corinti, D.; Crestoni, M. E.; Chiavarino, B.; Fornarini, S.; Scuderi, D.; Salpin, J.-Y. Insights into Cisplatin Binding to Uracil and Thiouracils from IRMPD Spectroscopy and Tandem Mass Spectrometry. *J. Am. Soc. Mass Spectrom.* **2020**, *31*, 946−960.
(36) Nieto, P.; Günther, A.; Berden, G.; Oomens, J.; Dopfer, O. IRMPD Spectroscopy of Metalated Flavins: Structure and Bonding of Lumiflavin Complexes with Alkali and Coinage Metal Ions. *J. Phys. Chem. A* **2016**, *120*, 8297−8308.
(37) Cismesia, A. P.; Bell, M. R.; Tesler, L. F.; Alves, M.; Polfer, N. C. Infrared Ion Spectroscopy: An Analytical Tool for the Study of Metabolites. *Analyst* **2018**, *143*, 1615−1623.
(38) Corinti, D.; Maccelli, A.; Crestoni, M. E.; Cesa, S.; Quaglio, D.; Botta, B.; Ingallina, C.; Mannina, L.; Tintaru, A.; Chiavarino, B.; Fornarini, S. IR Ion Spectroscopy in a Combined Approach with MS/MS and IM-MS to Discriminate Epimeric Anthocyanin Glycosides (Cyanidin 3-O-Glucoside and -Galactoside). *Int. J. Mass Spectrom.* **2019**, *444*, No. 116179.
(39) Corinti, D.; Maccelli, A.; Chiavarino, B.; Maitre, P.; Scuderi, D.; Bodo, E.; Fornarini, S.; Crestoni, M. E. Vibrational Signatures of Curcumin's Chelation in Copper(II) Complexes: An Appraisal by IRMPD Spectroscopy. *J. Chem. Phys.* **2019**, *150*, No. 165101.
(40) Martens, J.; van Outersterp, R. E.; Vreeken, R. J.; Cuyckens, F.; Coene, K. L. M.; Engelke, U. F.; Kluijtmans, L. A. J.; Wevers, R. A.; Buydens, L. M. C.; Redlich, B.; et al. Infrared Ion Spectroscopy: New Opportunities for Small-Molecule Identification in Mass Spectrometry - A Tutorial Perspective. *Anal. Chim. Acta* **2020**, *1093*, 1−15.
(41) Carlo, M. J.; Patrick, A. L. Infrared Multiple Photon Dissociation (IRMPD) Spectroscopy and Its Potential for the Clinical Laboratory. *J. Mass Spectrom. Adv. Clin. Lab.* **2022**, *23*, 14−25.
(42) Marshall, A. G.; Hendrickson, C. L.; Jackson, G. S. Fourier Transform Ion Cyclotron Resonance Mass Spectrometry: A Primer. *Mass Spectrom. Rev.* **1998**, *17*, 1−35.
(43) Bouchoux, G.; Salpin, J.-Y.; Leblanc, D. A Relationship between the Kinetics and Thermochemistry of Proton Transfer Reactions in the Gas Phase. *Int. J. Mass Spectrom. Ion Process.* **1996**, *153*, 37−48.
(44) Lemaire, J.; Boissel, P.; Heninger, M.; Mauclaire, G.; Bellec, G.; Mestdagh, H.; Simon, A.; Le Caer, S.; Ortega, J. M.; Glotin, F.; Maitre, P. Gas Phase Infrared Spectroscopy of Selectively Prepared Ions. *Phys. Rev. Lett.* **2002**, *89*, 273001−273002.
(45) Bakker, J. M.; Besson, T.; Lemaire, J.; Scuderi, D.; Maître, P. Gas-Phase Structure of a π-Allyl−Palladium Complex: Efficient Infrared Spectroscopy in a 7 T Fourier Transform Mass Spectrometer. *J. Phys. Chem. A* **2007**, *111*, 13415−13424.
(46) Oomens, J.; Sartakov, B. G.; Meijer, G.; von Helden, G. Gas-Phase Infrared Multiple Photon Dissociation Spectroscopy of Mass-Selected Molecular Ions. *Int. J. Mass Spectrom.* **2006**, *254*, 1−19.
(47) Prell, J. S.; O'Brien, J. T.; Williams, E. R. IRPD Spectroscopy and Ensemble Measurements: Effects of Different Data Acquisition and Analysis Methods. *J. Am. Soc. Mass Spectrom.* **2010**, *21*, 800−809.
(48) Zhao, Y.; Truhlar, D. G. The M06 Suite of Density Functionals for Main Group Thermochemistry, Thermochemical Kinetics, Noncovalent Interactions, Excited States, and Transition Elements: Two New Functionals and Systematic Testing of Four M06-Class Functionals and 12 Other Function. *Theor. Chem. Acc.* **2008**, *120*, 215−241.
(49) Chai, J.-D.; Head-Gordon, M. Long-Range Corrected Hybrid Density Functionals with Damped Atom−Atom Dispersion Corrections. *Phys. Chem. Chem. Phys.* **2008**, *10*, 6615−6620.
(50) Vydrov, O. A.; Scuseria, G. E.; Perdew, J. P. Tests of Functionals for Systems with Fractional Electron Number. *J. Chem. Phys.* **2007**, *126*, No. 154109.
(51) Vreven, T.; Frisch, M. J.; Kudin, K. N.; Schlegel, H. B.; Morokuma, K. Geometry Optimization with QM/MM Methods II: Explicit Quadratic Coupling. *Mol. Phys.* **2006**, *104*, 701−714.
(52) Vydrov, O. A.; Scuseria, G. E. Assessment of a Long-Range Corrected Hybrid Functional. *J. Chem. Phys.* **2006**, *125*, No. 234109.
(53) Yanai, T.; Tew, D. P.; Handy, N. C. A New Hybrid Exchange−Correlation Functional Using the Coulomb-Attenuating Method (CAM-B3LYP). *Chem. Phys. Lett.* **2004**, *393*, 51−57.
(54) Grimme, S.; Antony, J.; Ehrlich, S.; Krieg, H. A Consistent and Accurate Ab Initio Parametrization of Density Functional Dispersion Correction (DFT-D) for the 94 Elements H-Pu. *J. Chem. Phys.* **2010**, *132*, No. 154104.
(55) Becke, A. D.; Johnson, E. R. Exchange-Hole Dipole Moment and the Dispersion Interaction Revisited. *J. Chem. Phys.* **2007**, *127*, No. 154108.

https://doi.org/10.1021/acsomega.2c01236
ACS Omega 2022, 7, 19535−19544

(56) Barone, V.; Biczysko, M.; Bloino, J. Fully Anharmonic IR and Raman Spectra of Medium-Size Molecular Systems: Accuracy and Interpretation. *Phys. Chem. Chem. Phys.* **2014**, *16*, 1759−1787.
(57) Barone, V.; Cossi, M. Quantum Calculation of Molecular Energies and Energy Gradients in Solution by a Conductor Solvent Model. *J. Phys. Chem. A* **1998**, *102*, 1995−2001.
(58) Cossi, M.; Rega, N.; Scalmani, G.; Barone, V. Energies, Structures, and Electronic Properties of Molecules in Solution with the C-PCM Solvation Model. *J. Comput. Chem.* **2003**, *24*, 669−681.
(59) Zheng, Z.; Attygalle, A. B. Impact of Ambient Vapors Present in an Electrospray Ionization Source on Gas-Phase Ion Structures. *J. Am. Soc. Mass Spectrom.* **2021**, *32*, 725−735.
(60) Tian, Z.; Kass, S. R. Does electrospray ionization produce gas phase or liquid-phase structures? *J. Am. Chem. Soc.* **2008**, *130*, 10842−10843.
(61) Kumar, R.; Yerabolu, R.; Kenttamaa, H. I. Effects of residual water in a linear quadrupole ion trap on the protonation sites of 4-aminobenzoic acid. *J. Am. Soc. Mass Spectrom.* **2020**, *31*, 124−131.
(62) Zhang, H.-Y.; Wang, L. Solvent Effects are Important in Elucidating Radical Scavenging Mechanisms of Antioxidants. A Case Study on Genistein. *J. Biomol. Struct. Dyn.* **2005**, *22*, 483−486.
(63) Frisch, M. J.; Trucks, G. W.; Schlegel, H. B.; Scuseria, G. E.; Robb, M. A.; Cheeseman, J. R.; Scalmani, G.; Barone, V.; Mennucci, B.; Petersson, G. A.. *Gaussian 09*. Revision D.01; Gaussian Inc.: Wallingford, CT, USA, 2009.
(64) Liigand, P.; Kaupmees, K.; Kruve, A. Ionization Efficiency of Doubly Charged Ions Formed from Polyprotic Acids in Electrospray Negative Mode. *J. Am. Soc. Mass Spectrom.* **2016**, *27*, 1211−1218.
(65) Armentrout, P. B. Guided Ion Beam Studies of Transition Metal−Ligand Thermochemistry. *Int. J. Mass Spectrom.* **2003**, *227*, 289−302.
(66) Fabre, N.; Rustan, I.; de Hoffmann, E.; Quetin-Leclercq, J. Determination of Flavone, Flavonol, and Flavanone Aglycones by Negative Ion Liquid Chromatography Electrospray Ion Trap Mass Spectrometry. *J. Am. Soc. Mass Spectrom.* **2001**, *12*, 707−715.
(67) March, R. E.; Miao, X.-S.; Metcalfe, C. D.; Stobiecki, M.; Marczak, L. A Fragmentation Study of an Isoflavone Glycoside, Genistein-7-O-Glucoside, Using Electrospray Quadrupole Time-of-Flight Mass Spectrometry at High Mass Resolution. *Int. J. Mass Spectrom.* **2004**, *232*, 171−183.
(68) Wang, L.; Yang, F.; Zhao, X.; Li, Y. Effects of Nitro- and Amino-Group on the Antioxidant Activity of Genistein: A Theoretical Study. *Food Chem.* **2019**, *275*, 339−345.
(69) Sekine, R.; Robertson, E. G.; McNaughton, D. Raman, Infrared and Computational Analysis of Genistein and Its Methoxy Derivatives. *Vib. Spectrosc.* **2011**, *57*, 306−314.
(70) Zhang, J.; Du, F.; Peng, B.; Lu, R.; Gao, H.; Zhou, Z. Structure, electronic properties, and radical scavenging mechanisms of daidzein, genistein, formononetin, and biochanin A: A density functional study. *J. Mol. Struct.: THEOCHEM* **2010**, *955*, 1−6.
(71) Katari, M.; Duncan Carmichael, D.; Jacquemin, D.; Frison, G. Structure of electronically reduced N-donor bidentate ligands and their heteroleptic four-coordinate zinc complexes: a survey of density functional theory results. *Inorg. Chem.* **2019**, *58*, 7169−7179.
(72) Rodrigues-Oliveira, A. F.; Ribeiro, F. W. M.; Cervi, G.; Correra, T. C. Evaluation of Common Theoretical Methods for Predicting Infrared Multiphotonic Dissociation Vibrational Spectra of Intramolecular Hydrogen-Bonded Ions. *ACS Omega* **2018**, *3*, 9075−9085.
(73) Fornaro, T.; Biczysko, M.; Monti, S.; Barone, V. Dispersion Corrected DFT Approaches for Anharmonic Vibrational Frequency Calculations: Nucleobases and Their Dimers. *Phys. Chem. Chem. Phys.* **2014**, *16*, 10112−10128.
(74) Oomens, J.; Steill, J. D.; Redlich, B. Gas-Phase IR Spectroscopy of Deprotonated Amino Acids. *J. Am. Chem. Soc.* **2009**, *131*, 4310−4319.

https://doi.org/10.1021/acsomega.2c01236
ACS Omega 2022, 7, 19535−19544